Gradient-Index Granular Crystals: From Boomerang Motion to Asymmetric Transmission of Waves

Eunho Kim,[1,2,3] Rajesh Chaunsali,[1] and Jinkyu Yang[1,*]
[1]Aeronautics and Astronautics, University of Washington, Seattle, Washington 98195-2400, USA
[2]Division of Mechanical System Engineering, Jeonbuk National University, 567 Baekje-daero, Deokjin-gu, Jeonju-si, Jeollabuk-do, Republic of Korea 54896
[3]Automotive Hi-Technology Research Center & LANL-CBNU Engineering Institute-Korea, Jeonbuk National University, 567 Baekje-daero, Deokjin-gu, Jeonju-si, Jeollabuk-do, Republic of Korea 54896

(Received 24 June 2019; published 18 November 2019)

We present a gradient-index crystal that offers extreme tunability in terms of manipulating the propagation of elastic waves. For small-amplitude excitations, we achieve control over wave transmission depth into the crystal. We numerically and experimentally demonstrate a boomeranglike motion of a wave packet injected into the crystal. For large-amplitude excitations on the same crystal, we invoke nonlinear effects. We numerically and experimentally demonstrate asymmetric wave transmission from two opposite ends of the crystal. Such tunable systems can thus inspire a novel class of designed materials to control linear and nonlinear elastic wave propagation in multiscales.

DOI: 10.1103/PhysRevLett.123.214301

Introduction.—The advent of phononic crystals and metamaterials in recent years has shown excellent possibilities to manipulate elastic waves in materials [1–3]. Several ingenious designs have been proposed to build exotic devices, e.g., a diode [4–6], cloak [7], negative refraction metamaterial [8,9], energy harvester [10,11], impact absorber [12], flow stabilizer [13] and topological lattice [14,15]. The key idea is to use one or more ingredients among structural periodicity [16], local resonances [17], nonlinear effects [18], etc., to achieve nontrivial dynamical responses. The underlying physics in these demonstrations could also open new ways to control mechanical vibrations at the nanoscale by optomechanical [19] and nanophononic metamaterials [20]. Therefore, the need of exploring advanced material architectures that offer rich wave physics is ever growing.

In this context, granular crystals [21,22]—a systematic arrangement of granular particles—offer a unique advantage. These architectures mimic atomic lattice dynamics in the sense that the grains can be regarded as atoms that interact via a nonlinear interaction potential stemming from the nature of the contact. These crystals are highly tunable, and a plethora of wave physics can be demonstrated in the same system [23]. Control over wave propagation in this setting shows many technological advances, ranging from impact and blast protection [24] to microscale granular beds [25].

In this Letter, we present a *gradient-index* granular crystal that offers even further tunability in terms of manipulating both linear and nonlinear elastic waves. These granular particles are of a cylindrical shape, where simply by tuning the contact angles between them, a gradient in stiffness can be achieved [26]. Gradient-index materials have been extensively studied in optics and acoustics for various purposes, such as rainbow trapping [27], opening wide band gaps [28], waveguides [29,30], lens [31–34], beamwidth compressor [35], wave concentration [36], and absorbers [37,38]. Gradient-index systems are unique as the gradual variation in material or structural properties enables control over wave speed and wave directions at the same time minimizing wave scattering.

Using the gradient-index granular crystal, here, we numerically and experimentally demonstrate capability of wave control in two fronts. For small-amplitude waves, the system follows linear dynamics, and therefore, we demonstrate frequency-dependent wave penetration into the system. This includes a boomeranglike motion of injected wave packet that returns back to the point of excitation without propagating through the whole crystal. This is similar to a mirage effect. For large-amplitude waves, we invoke nonlinear effects [39–41], and we show that the system offers asymmetric wave transmission in two opposite directions. This leads to one-way energy transport as a result of the interaction of nonlinearity and spatial asymmetry [5,6,42–45]. Remarkably, all these characteristics can be tuned simply by changing the stacking angles and controlling the wave amplitude in the system.

Experimental and numerical setup.—Our system is composed of 37 cylinders (with the length and the diameter equal to 18 mm) stacked vertically and precompressed by a free weight on top as shown in Fig. 1. We vertically align the cylinders using 3D-printed cylindrical enclosures (lower inset of Fig. 1). Each enclosure has one cylinder inside, and deliberate clearances are provided to restrict

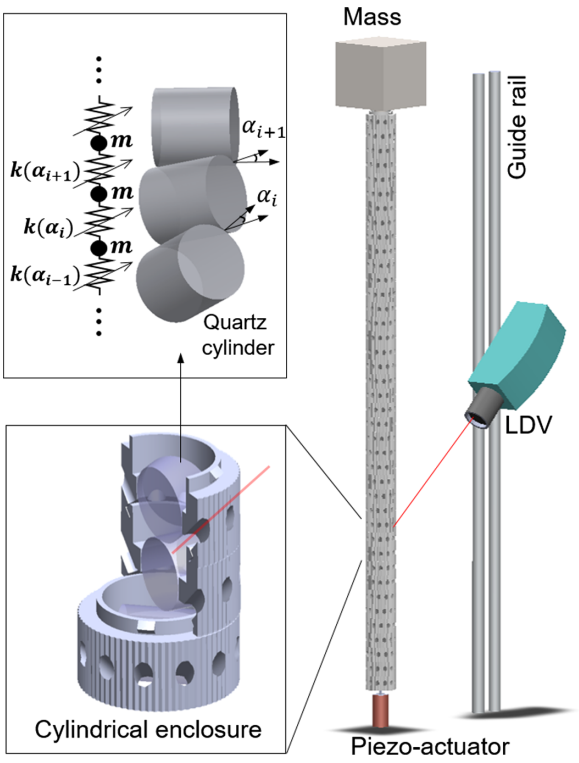

FIG. 1. Experiment setup to investigate wave dynamics in a gradient-index granular crystal.

their rattling in rotation and to minimize any friction in the translational direction. The enclosures are assembled in series and can be rotated independently to dial in contact angles between neighboring cylindrical particles inside. The cylinders interact as per the Hertz contact law [46], and therefore, linear (nonlinear) wave dynamics can be studied at small (large) dynamic excitations in comparison to the static precompressive force ($F_0 = 29.4$ N). We vary the contact angles ranging from 10° to 90° along the chain such that the contact stiffness varies linearly along the chain. 10° represents a stiff side, whereas 90° is a soft side. A piezoelectric actuator (Piezomechanik PSt 500/10/25 VS18) is placed at the bottom of the chain in contact with the first particle. The actuator excites the chain using a Gaussian wave packet with a specific central frequency. A function generator (Agilent 33220A) sends the input to the actuator via an amplifier (Piezomechanik LE 150/100 EBW). We measure velocity of each particle by a laser Doppler vibrometer (Polytec OFV-534) at 45° through the delicately designed holes in the enclosures. The point-by-point measurements of the particles are synchronized to reconstruct the wave field along the chain.

To investigate wave dynamics, we first numerically model the system by employing the discrete element method (upper inset of Fig. 1). Each fused-quartz cylinder (Young's modulus $E = 72$ GPa, Poisson's ratio $\nu = 0.17$, and density $\rho = 2200$ kg/m^3) is considered as a point mass having only one degree of freedom in the vertical direction. The interaction of the ith and $(i+1)$th cylinders—making a contact angle α_i—is modeled as the following force-displacement law: $F = \beta(\alpha_i)(\delta_i + u_i - u_{i+1})^{3/2}$. Here $\beta(\alpha_i)$ is the contact stiffness coefficient, u_i denotes the dynamic displacement of ith cylinder, and δ_i is the precompression due to the static force given to the system [see Supplemental Material [47] for the full expression of $\beta(\alpha_i)$ and equations of motion]. We neglect the gravitational force because it is much smaller compared to F_0. We explore the linear wave dynamics of the system by studying the modal response of the system. To this end, for small dynamical excitations, we can linearize our contact model such that contact stiffness $k_{\text{lin}}(\alpha_i) = (3/2)\beta(\alpha_i)^{2/3}F_0^{1/3}$.

Linear dynamics.—In Fig. 2(a), we show modal frequencies of lossless gradient-index chain (10° → 90°) in comparison to *homogeneous* chains (10° → 10° and

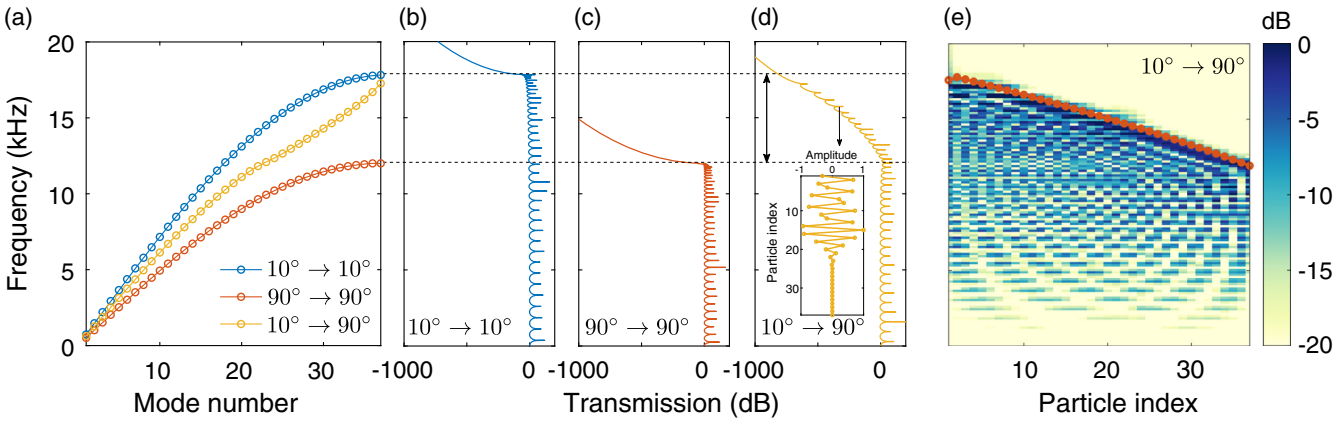

FIG. 2. Modal frequencies and transmission of the gradient-index granular chain in comparison to homogeneous chains. (a) Modal frequencies of a gradient-index chain with contact angle 10° → 90° along with the homogeneous chains with only 10° and 90°. (b)–(c) State-space-based wave transmission for the homogeneous chain with contact angle 10° and 90°. (d) The same for the gradient-index chain. (e) Frequency spectrum vs space obtained from full numerical simulations on the gradient-index chain under an impact excitation. The highlighted line in red represents analytically obtained *local* cutoff frequency.

90° → 90°), i.e., uniform contact angle (thus stiffness k_{lin}) along the length. We observe that the eigenfrequencies of the 10° → 10° chain span up to a cutoff frequency about 17.78 kHz [$= (1/\pi)\sqrt{k_{\mathrm{lin}}(10°)/m}$, where m represents the mass of cylinders and $k_{\mathrm{lin}}(10°)$ denotes linearized stiffness for 10° contact]. Similarly, for the 90° → 90° chain, we observe eigenfrequencies cover the spectrum up to 11.97 kHz [$= (1/\pi)\sqrt{k_{\mathrm{lin}}(90°)/m}$]. For the gradient-index chain, however, we observe eigenfrequencies extend to about 17.78 kHz (i.e., the cutoff frequency for 10° → 10° chain), but the curve has a portion that is concave upward starting from about 11.97 kHz (the cutoff frequency for 90° → 90° chain). These modes are referred to as "gradons" in the previous literature [48].

To investigate further, we plot the wave transmission as a function of frequency for all the aforementioned configurations in Figs. 2(b)–2(d). For this, we use state-space approach to calculate the ratio of output force (felt by the upper mass) to input force (by the lower actuator) [49]. It is evident that 10° → 10° and 90° → 90° homogeneous chains have pass bands from 0 kHz to their respective cutoff frequencies, whereas the gradient chain shows a pass band with decreasing transmission in the frequency range marked by the double-sided arrow in Fig. 2(d), which corresponds to the region with the concave upward trend in Fig. 2(a). We show in the inset a mode shape for a frequency in this region. Since its modal amplitude dominates the chain only partially, we can explain why the wave transmission decreases in this region.

We verify this argument further by performing full numerical simulation with a small-amplitude impulse excitation given to the chain (Runge-Kutta solver with 0.01 m/s of initial velocity to the first particle). We then perform the fast Fourier transformation (FFT) on the velocity time history of each particle to plot frequency spectrum along the length of the chain as shown in Fig. 2(e). We observe that the wave transmission is only partial along the chain in the frequency range mentioned above. As the input frequency increases in this region, the transmission is more limited to the front end of the chain. Therefore, we can interpret linear dynamics in this gradient-index chain as if the system has spatially varying "local" cutoff frequency. Analytical expression of such a local cutoff frequency can be mathematically expressed as $f_{c,i} = (1/\pi)\sqrt{k_{\mathrm{lin}}(\alpha_i)/m}$, which shows an excellent fit with the numerical results shown Fig. 2(e). We thus conclude that our gradient-index chain would have three regions of wave transmission. From 0 to 11.97 kHz, there is a pass band; from 11.97 to 17.78 kHz, there is a *quasistop* band, i.e., wave transmission up to a fraction of the chain; and for frequencies above 17.78 kHz, there is a stop band.

With the understanding of the three different regions of wave transmission in our gradient-index chain, we now send Gaussian-modulated waveforms centered at frequencies residing in these three regions. We numerically and experimentally show how the wave packet propagates along the chain when sent from the stiffer side (10°). In Figs. 3(a) and 3(b), we show spatiotemporal evolution of a wave packet at 7 kHz obtained numerically and experimentally. As the frequency falls in the region of full transmission, we clearly observe that the wave packet is transmitted to the other end of the chain. A significant decay in amplitude, however, is due to the damping in the experiments, which is modeled in simulations as well

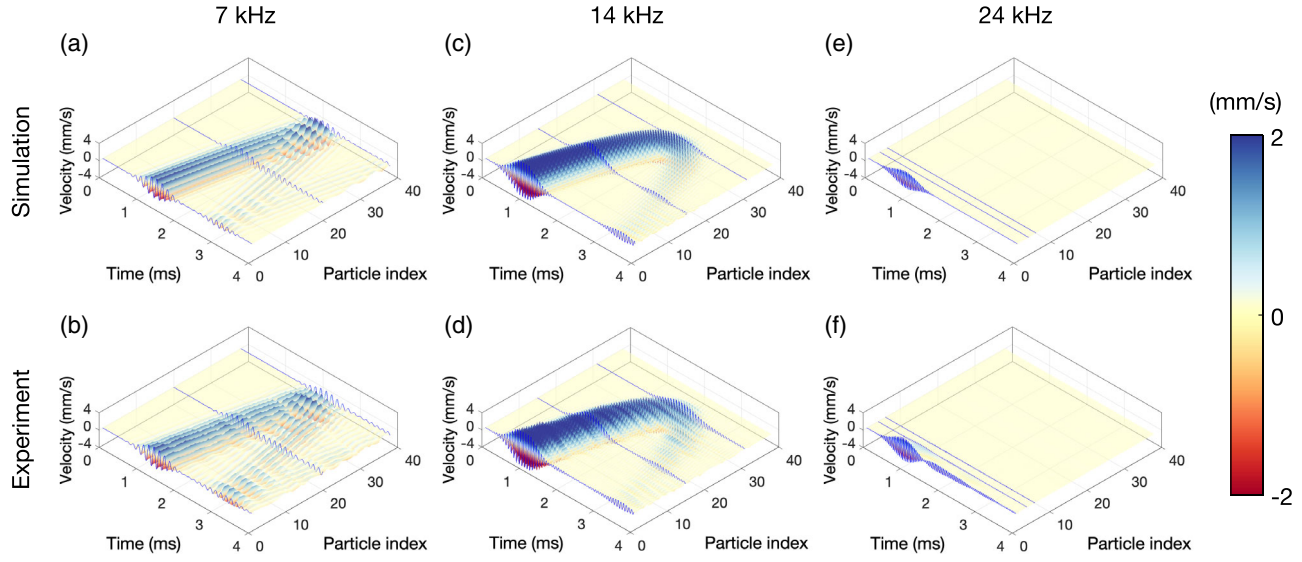

FIG. 3. Linear wave dynamics in the gradient-index chain (10° → 90°) under a Gaussian-modulated wave excitation. (a)–(b) Numerically and experimentally obtained spatiotemporal velocity maps for the excitation centered at 7 kHz. 3D line plots (in blue) are superimposed to highlight velocity time history at certain locations along the chain. (c)–(d) The same at 14 kHz with the boomeranglike wave propagation. (e)–(f) The same at 24 kHz.

(Supplemental Material [47]). In Figs. 3(c) and 3(d), we show spatiotemporal evolution of a wave packet at 14 kHz, which lies in the partial wave transmission region. Evidently, the wave packet slows down as it propagates along the chain. It stops at a spatial location and then turns back to the front of the chain. This is analogous to boomerang motion, which we could successfully capture in our experiments. This boomerang motion typically involves wave amplification near the turning location (Supplemental Material [47]). Lastly, the wave sent at 24 kHz in the stop band does not propagate along the chain at all and is confined to the left end [Figs. 3(e) and 3(f)]. In this way, we have demonstrated that our gradient-index system offers great control over the penetration depth of the wave packet as a function of its frequency.

Nonlinear dynamics.—We now investigate wave dynamics for larger amplitudes by invoking nonlinear effects. In particular, we consider the frequency regime that offers partial wave transmission, the uniqueness of this gradient-index chain, and then increase wave amplitude to assess transmission characteristics of the system. We send a Gaussian-modulated pulse centered at 13.5 kHz from the two opposite ends and numerically monitor wave transmission as shown in Fig. 4. We quantify wave transmission as the ratio of the maximum velocity of the last particle to that of the first particle. Viscous damping is ignored here. For small-amplitude excitations, the forward configuration (10° → 90°) shows boomerang wave motion and returns back without reaching the other end as predicted earlier. However, upon increasing the wave amplitude, we see a significant rise in wave transmission through the chain due to wave leakage as seen in the upper panels of Fig. 4.

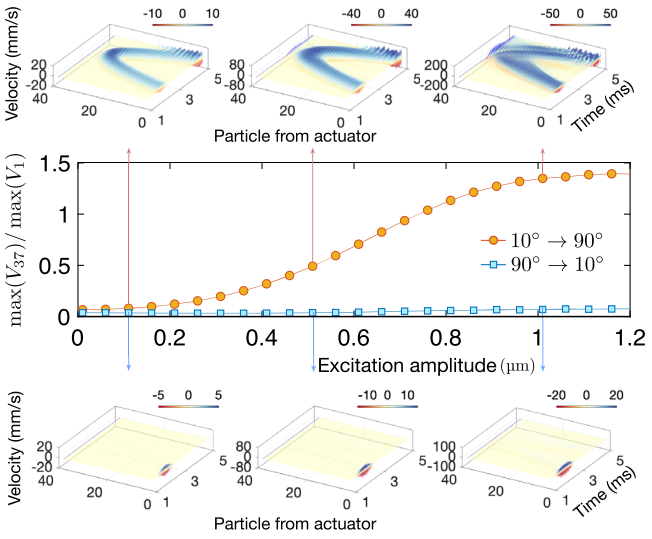

FIG. 4. Nonlinear wave dynamics in the gradient-index granular crystal. We observe asymmetry in wave transmission with increasing excitation amplitude from 0.11 (left panel), 0.51 (middle), to 1.01 μm (right), at 13.5 kHz for two configurations: forward (10° → 90°, top panel) and reverse (90° → 10°, bottom).

In contrast, for the reverse configuration (90° → 10°), the wave does not penetrate the bulk of the chain and remains localized near the excitation point as seen in the bottom panels of Fig. 4. Upon increasing the wave amplitude, the localization still persists, and there is not a significant rise in the wave transmission.

This amplitude-dependent asymmetric wave transmission can be understood as the interplay between nonlinearity and spatial gradient in the system. Looking back at the eigenmode (gradon) plotted in the inset in Fig. 2(d), when we excite the system from the stiffer side (10°), the presence of larger modal amplitude contributes to invoking nonlinear effects (such as frequency shifts) easily with an increased excitation amplitude. However, when we excite the system from the soft side (90°), nonlinear effects become substantially suppressed, similar to the mechanism observed in thermal systems [42]. By further investigating this phenomenon in the frequency spectra for both small and large excitation amplitudes, we observe that the enhancement of the wave transmission in the forward configuration is due to the *gradual* frequency softening and spatial extension of the nonlinear mode (Supplemental Material [47]). We note that this mechanism is different from those relying on harmonic generation [5], bifurcation [6], or self-demodulation [43].

Next, we experimentally demonstrate the asymmetric wave transmission in our gradient-index chain. We send a Gaussian-modulated pulse used in Fig. 4 from the actuator

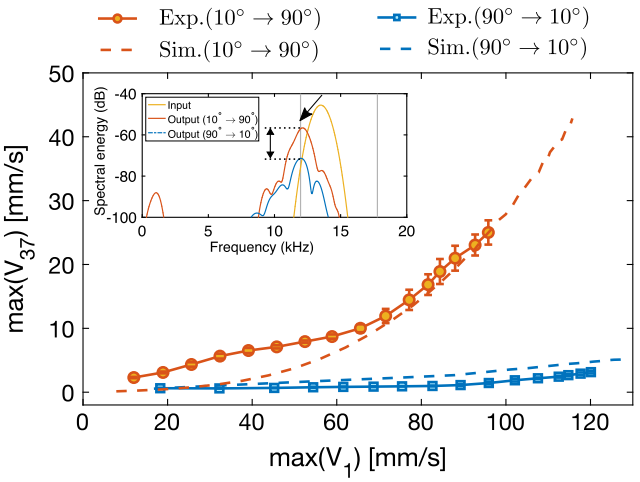

FIG. 5. Comparison of asymmetric wave transmission data obtained from experiments and numerical simulations for two configurations: forward (10° → 90°) and reverse (90° → 10°). The maximum velocity of the last (37th) particle from the actuator is compared with various excitation amplitude of the first particle from the actuator. Inset shows the experimentally obtained frequency content at the output of the chain. Two vertical gray lines denote the region of local cutoff frequencies in the chain. The arrow indicates the frequency shift from the input to the lowest local cutoff frequency. Double-sided arrow denotes the magnitude of asymmetry.

to the two different configurations: forward (10° → 90°) and reverse (90° → 10°), and measure wave transmission. In Fig. 5, we show the experimental evidence of asymmetric transmission in our system when the excitation amplitude is increased. The numerical simulation, which also includes the effect of viscous damping, follows the experimental data with a decent agreement. The inset highlights the aforementioned frequency shift governed by the local cutoff frequencies, and thereby leading to asymmetric wave transmission of about 15 dB. Note that the excitation range in the experiments is narrower than that in the simulations due to the limitation of our piezoelectric stack actuator. However, the asymmetric transmission is clearly verified within the range covered.

Conclusion.—We have proposed a highly tunable gradient-index system that is made of cylindrical granules. The contact interaction allows us to easily maintain a stiffness gradient along the chain. Because of the nonlinear Hertz contact law, the system is further tunable by the amplitude of wave excitation. For small amplitudes, the system follows linear dynamics and shows three distinctive frequency regions of wave transmission. These are a stop band, a pass band, and a quasistop band, which allows waves to penetrate only to a fraction of the system and then return back to the point of excitation. We experimentally demonstrate such a boomerang motion. For high amplitude excitations, we invoke nonlinear effects (gradual frequency softening) in the system, and demonstrate that the same system supports asymmetric wave transmission, leading to a rapid enhancement of transmission from one end to the other. Therefore, this contact-based tunable system can inspire novel class of systems to manipulate the flow of elastic energy for engineering applications, e.g., impact mitigation, vibration filtering, energy harvesting, and even mechanical logic gates. The underlying nonlinear mechanism of our system can also stimulate future studies in other domains such as plasmonics and photonics.

We thank Panayotis Kevrekidis (University of Massachusetts, Amherst) and Georgios Theocharis (CNRS) for valuable suggestions. E. K. acknowledges the support from the National Research Foundation of Korea, NRF-2017R1C1B5018136. J. Y. is grateful for the support of the National Science Foundation under Grant No. CAREER-1553202.

*jkyang@aa.washington.edu

[1] M. Maldovan, Nature (London) **503**, 209 (2013).
[2] M. Kadic, T. Bückmann, R. Schittny, and M. Wegener, Rep. Prog. Phys. **76**, 126501 (2013).
[3] M. I. Hussein, M. J. Leamy, and M. Ruzzene, Appl. Mech. Rev. **66**, 040802 (2014).
[4] B. Li, L. Wang, and G. Casati, Phys. Rev. Lett. **93**, 184301 (2004).
[5] B. Liang, B. Yuan, and J.-c. Cheng, Phys. Rev. Lett. **103**, 104301 (2009).
[6] N. Boechler, G. Theocharis, and C. Daraio, Nat. Mater. **10**, 665 (2011).
[7] M. Farhat, S. Guenneau, and S. Enoch, Phys. Rev. Lett. **103**, 024301 (2009).
[8] X. Zhang and Z. Liu, Appl. Phys. Lett. **85**, 341 (2004).
[9] R. Zhu, X. N. Liu, G. K. Hu, C. T. Sun, and G. L. Huang, Nat. Commun. **5**, 5510 (2014).
[10] S. Yang, J. H. Page, Z. Liu, M. L. Cowan, C. T. Chan, and P. Sheng, Phys. Rev. Lett. **93**, 024301 (2004).
[11] M. Carrara, M. R. Cacan, J. Toussaint, M. J. Leamy, M. Ruzzene, and A. Erturk, Smart Mater. Struct. **22**, 065004 (2013).
[12] C. Daraio, V. F. Nesterenko, E. B. Herbold, and S. Jin, Phys. Rev. Lett. **96**, 058002 (2006).
[13] M. I. Hussein, S. Biringen, O. R. Bilal, and A. Kucala, Proc. R. Soc. A **471**, 20140928 (2015).
[14] P. Wang, L. Lu, and K. Bertoldi, Phys. Rev. Lett. **115**, 104302 (2015).
[15] G. Ma, M. Xiao, and C. T. Chan, Nat. Rev. Phys. **1**, 281 (2019).
[16] L. Brillouin, *Wave Propagation in Periodic Structures*, 2nd ed. (Dover Publications, New York, 1953).
[17] Z. Liu, X. Zhang, Y. Mao, Y. Y. Zhu, Z. Yang, C. T. Chan, and P. Sheng, Science **289**, 1734 (2000).
[18] C. Chong, M. A. Porter, P. G. Kevrekidis, and C. Daraio, J. Phys. Condens. Matter **29**, 413003 (2017).
[19] M. Eichenfield, J. Chan, R. M. Camacho, K. J. Vahala, and O. Painter, Nature (London) **462**, 78 (2009).
[20] B. L. Davis and M. I. Hussein, Phys. Rev. Lett. **112**, 055505 (2014).
[21] V. Nesterenko, *Dynamics of Heterogeneous Materials*, 1st ed. (Springer-Verlag, New York, 2001).
[22] S. Sen, J. Hong, J. Bang, E. Avalos, and R. Doney, Phys. Rep. **462**, 21 (2008).
[23] M. A. Porter, P. G. Kevrekidis, and C. Daraio, Phys. Today **68**, No. 11, 44 (2015).
[24] E. Kim, Y. H. N. Kim, and J. Yang, Int. J. Solids Struct. **58**, 128 (2015).
[25] M. Hiraiwa, M. Abi Ghanem, S. P. Wallen, A. Khanolkar, A. A. Maznev, and N. Boechler, Phys. Rev. Lett. **116**, 198001 (2016).
[26] D. Khatri, D. Ngo, and C. Daraio, Granular Matter **14**, 63 (2012).
[27] K. L. Tsakmakidis, A. D. Boardman, and O. Hess, Nature (London) **450**, 397 (2007).
[28] M. S. Kushwaha, B. Djafari-Rouhani, L. Dobrzynski, and J. O. Vasseur, Eur. Phys. J. B **3**, 155 (1998).
[29] H. Kurt and D. S. Citrin, Opt. Express **15**, 1240 (2007).
[30] Z. He, F. Cai, and Z. Liu, Solid State Commun. **148**, 74 (2008).
[31] D. R. Smith, J. J. Mock, A. F. Starr, and D. Schurig, Phys. Rev. E **71**, 036609 (2005).
[32] D. Torrent and J. Sánchez-Dehesa, New J. Phys. **9**, 323 (2007).
[33] S. A. R. Horsley, I. R. Hooper, R. C. Mitchell-Thomas, and O. Quevedo-Teruel, Sci. Rep. **4**, 4876 (2014).
[34] Y. Jin, R. Kumar, O. Poncelet, O. Mondain-Monval, and T. Brunet, Nat. Commun. **10**, 143 (2019).

[35] S.-C. S. Lin, B. R. Tittmann, J.-H. Sun, T.-T. Wu, and T. J. Huang, J. Phys. D **42**, 185502 (2009).
[36] V. Romero-García, R. Picó, A. Cebrecos, V. J. Sánchez-Morcillo, and K. Staliunas, Appl. Phys. Lett. **102**, 091906 (2013).
[37] A. Climente, D. Torrent, and J. Sánchez-Dehesa, Appl. Phys. Lett. **100**, 144103 (2012).
[38] Y.-J. Liang, L.-W. Chen, C.-C. Wang, and I.-L. Chang, J. Appl. Phys. **115**, 244513 (2014).
[39] R. K. Narisetti, M. J. Leamy, and M. Ruzzene, J. Vib. Acoust. **132**, 031001 (2010).
[40] R. Ganesh and S. Gonella, Wave Motion **50**, 821 (2013).
[41] M. H. Abedinnasab and M. I. Hussein, Wave Motion **50**, 374 (2013).
[42] N. Yang, N. Li, L. Wang, and B. Li, Phys. Rev. B **76**, 020301(R) (2007).
[43] T. Devaux, V. Tournat, O. Richoux, and V. Pagneux, Phys. Rev. Lett. **115**, 234301 (2015).
[44] Z. Wu, Y. Zheng, and K. W. Wang, Phys. Rev. E **97**, 022209 (2018).
[45] K. J. Moore, J. Bunyan, S. Tawfick, O. V. Gendelman, S. Li, M. Leamy, and A. F. Vakakis, Phys. Rev. E **97**, 012219 (2018).
[46] K. L. Johnson, *Contact Mechanics* (Cambridge University Press, Cambridge, England, 1985).
[47] See Supplemental Material at http://link.aps.org/supplemental/10.1103/PhysRevLett.123.214301 for details on numerical modeling, wave amplification in linear dynamics, frequency conversion associated with nonlinear dynamics, and the effect of the stiffness gradient profile, which includes Refs. [26,46].
[48] J. J. Xiao, K. Yakubo, and K. W. Yu, Phys. Rev. B **73**, 054201 (2006).
[49] N. Boechler, J. Yang, G. Theocharis, P. G. Kevrekidis, and C. Daraio, J. Appl. Phys. **109**, 074906 (2011).